KELVIN–HELMHOLTZ INSTABILITY ON SHOCK PROPAGATION IN CURVED CHANNEL

I.E. IVANOV[1], J.N. DOWSE[2], I.A., KRYUKOV[1], B.W. SKEWS[2], I.A. ZNAMENSKAYA[1]

[1]Department of Physics, Lomonosov State University, Moscow, 119991, Russia

[2]The University of the Witwatersrand Johannesburg, Wits 2050, South Africa

[c]Corresponding author: Tel.: + 7(495)939-44-28; Email: znamen@phys.msu.ru

Introduction

Kelvin–Helmholtz instability (KHI) was observed in some gas dynamic flows with shock waves when velocity shear is within a fluid. Experimental results for shock interaction with curved channel profile had been obtained [1]. Accurate analysis of the problem in channel with 80% area reduction showed that in later time steps shear layers break down and form large KH instabilities. A color Schlieren technique was used; high accuracy was achieved in space resolution of flow visualization. In the reduced section the results show earlier produced sets of shear layers breaking down into KHI, later it becomes quite intense near the boundary.
Detailed high performance computing was conducted for the 2D analysis of the problem. The objective was to discover the starting point of KHI arising. Initial Mach number was 1,2-2. The two-dimensional unsteady Euler equations and Navier-Stokes equations were solved with finite-volume Godunov method of high order. MUSCL approach was implemented with the procedure of the spatial reconstruction of the conservative fifth-order accuracy in conjunction with the Runge-Kutta third-order approximation in time. Numerical calculations were performed on a uniform Cartesian computational grid of computational cells 4800x1200.
In the presented paper for the analysis of shock-wave configurations arising in the shock wave diffraction on the reduction area, the approach for shock waves reflection from a wedge [2-5] is developed.

Profile Geometric Description

The curve configuration used to describe the overall area reduction as shown in Figure 1. It consists of the two walls with reductions symmetrical about the y-axis. Each wall reduction is defined by two parabolic curves, vertical axis of symmetry, one with a positive gradient and other with a negative gradient. The turning points are at the beginning and end of the wall reduction respectively. The two parabolic curves intersect at a point of inflection located with a y-coordinate midway along the profile length.

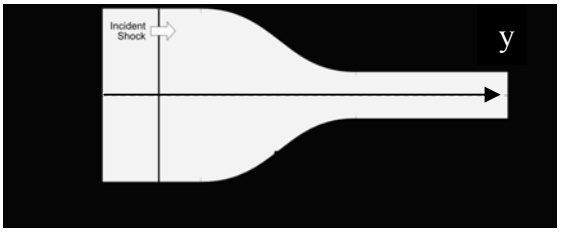

Fig.1. Flow profile.

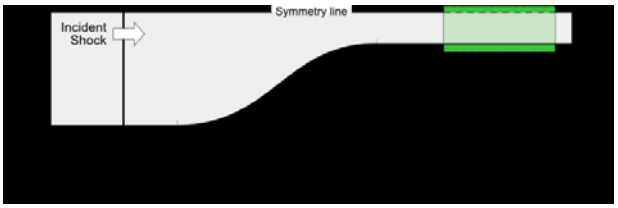

Fig. 2. Domain for CFD simulation.

The investigated configuration involves an 80% reduction in area with a profile length of 130mm. The dimensions used for computational analysis are given as follows in Figure 1. The area of interest is the complex flow degradation which typically occurs in area A as shown in Fig. 2.

Computational Fluid Dynamics

As the mathematical model for flow simulation (for two-dimensional unsteady compressible flow of a perfect gas), we took the system of 2D time-dependent Navier-Stokes (and also Euler) equations [6-8], with the corresponding boundary conditions. Upper and lower boundaries were rigid non-penetrable walls. Adiabatic conditions were used for the walls. Supersonic flow conditions were set at inlet section; non-reflecting conditions were set for outlet section.
The computations were carried out using a finite volume Godunov-type method. The flux terms were evaluated by an exact Riemann solver. Time advancement is achieved using a third-order TVD Runge-Kutta method [9]. High-order spatial accuracy is achieved using fifth order MUSCL reconstruction.. The slopes are calculated using a fifth order polynomial reconstruction with a limited first derivative. The fourth-order approximation [10] is used for the first derivative. The approximation includes a limitation that enforces to satisfy the condition that first derivative is equal to zero near an extremum. CFD calculations were performed at various grid point numbers. After grid convergence studies, a grid was selected. Accuracy of numerical scheme was up to fifth order. The fifth-order reconstruction gives significantly better resolution than classic second order reconstructions, especially for contact surfaces.

The most acceptable parameters for typical simulations were 4800x1200 grid points at the fifth-order numerical scheme accuracy. Calculations (a solution of Euler's) were conducted for the entire area, and for symmetric half-zone.

Good qualitative and also quantitative agreement of the 2D CFD simulation with experimental data was achieved.

Numerical simulation of shock wave diffraction on curvilinear compression corner in channel.

The problem being solved was: a plane shock wave M=1.33 interacts with a curvilinear contraction in the channel. Numerical simulation result analysis allows outlining several essential diffraction stages. In the early stage the interaction realizes as the nonregular reflection, at first it is the simple Mach reflection and then it is the double Mach reflection. When the incident shock wave approaches the zone of maximal curvilinear wall contour gradient the shock wave reflection becomes more complex. Fig.3 schematically shows the shock-wave flow structure in the upper half of the channel. Here and further we use the following notation: I_i - incident shock wave, R_i - reflected shock wave, M_i - Mach stem, C_i - contact discontinuity, T_i - main triple point. Directions of gas dynamical discontinuities are shown with arrows, the line CD corresponds to the channel wall and AB corresponds to the symmetry plane. Subscript designates the number of shock-wave structure that is generated as result of reflected shock wave interaction with the wall or symmetry plane. The reflection type doesn't change after the Mach reflection shock-wave structure generation and further incident shock wave propagation till the curvilinear wall contour gradient decreases and becomes zero. The maximal declination angle of the curvilinear wall to the symmetry line achieves in the middle of the curvilinear part and is equal to 36.4 degrees. The reflected wave R_1 has complex structure in the time of the shock wave interaction with the wall. It consists of a rarefaction fan that transfers to a shock wave near the triple point T_1. The shock wave part of R_1 increases as far as the incident wave propagates to the right and the reflected wave propagates down. As result the triple point T_1 moves along some trajectory directed from top to bottom and from left to right.

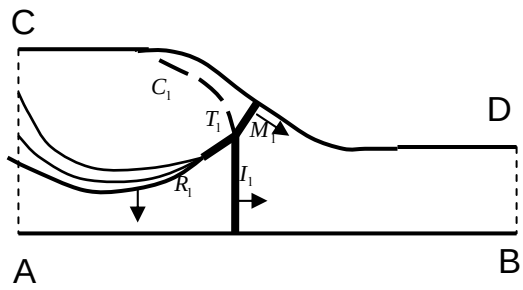

Fig.3.

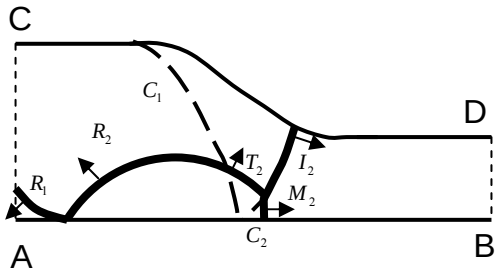

Fig. 4

The wave R_1 reflects from the symmetry plane AB as the shock wave R_2 and rarefaction fan (fig.5a). Two coupling points s_1 and s_2 of two branches of the reflected wave R_1 and R_2 move along AB in different directions. The point s_2 moves to the right in the direction of the incident shock wave and catches up the wave as the branches of shock wave R_1 and the triple point T_1 approach the symmetry plane AB. After "collapse" of the triangular zone between points T_1 s_1 j_1 (fig.5b) the segment of the incident shock wave I_1 disappears and the Mach stem M_1 turn into a new incident wave $I_2 = M_1$ after that.

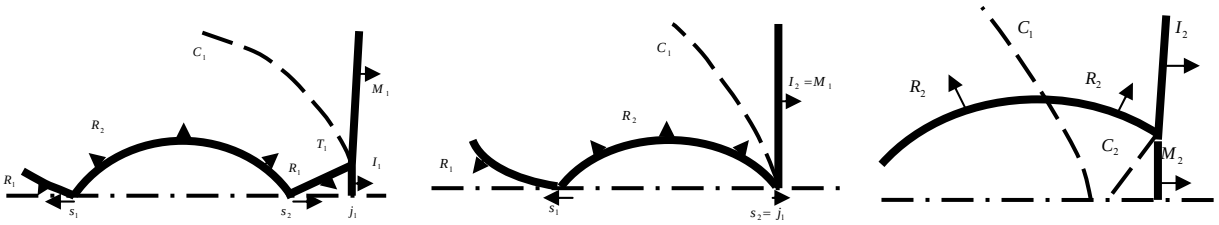

a b c

Fig. 5 Sketch of shock-wave structures at the shock reflection from the symmetry plane.

The reflected shock wave R_2 propagates up and its intersection with I_2 produces the new triple point T_2. The new Mach stem M_2 is located below this point and I_2 is located above it (fig.3c). The C_2, which leaves the triple point T_2, turns down and left relative to the symmetry plane. The contact discontinuity C_1 connected with the structures that are generated in the process of the reflection from the wall "comes off" from the second level shock-wave structure I_2 M_2 R_2 and terminates near the symmetry plane.

Fig.6 shows the isolines of the density flowfield just before the triple point T_1 reaches the axis of symmetry, (a); at the time of contact (b), and after a full reflection R_1 of the plane of symmetry and the formation of the shock wave structure I_2 M_2 R_2 (c).

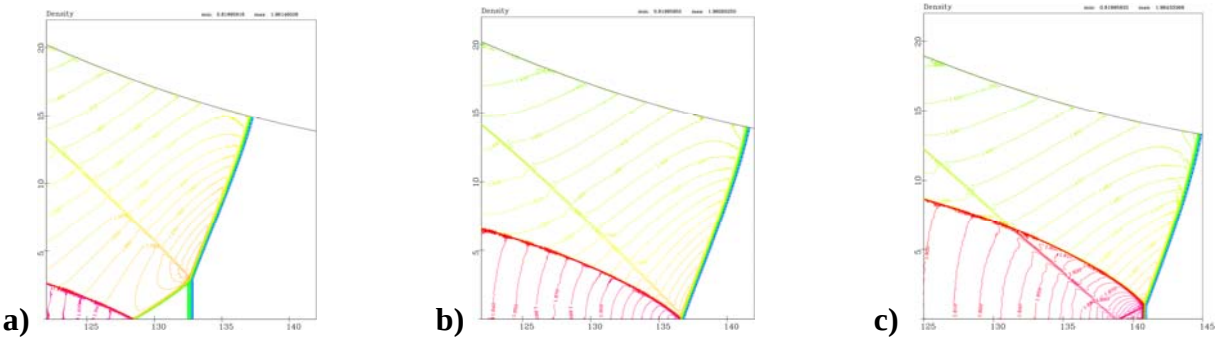

Fig. 6. Isolines of the density at the shock wave R_1 reflection from the plane of symmetry.

The structure of the flow after the transverse wave R_1 reflection on the plane of symmetry is shown schematically in fig. 4 and in fig. 7 (isolines of the density field).

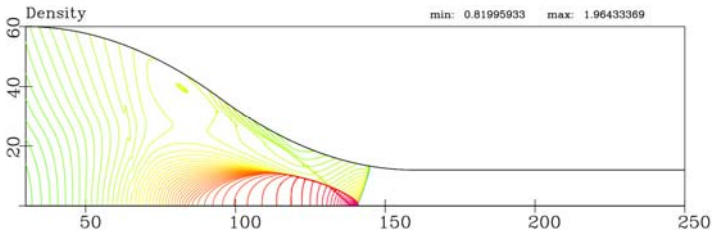

Fig. 7

At the subsequent moments of time C_1 with gas flow, which moves to the right behind the shock-wave structure $I_2\ M_2\ R_2$ (fig.2, fig.3c). Thus the line C_1 remains a line of contact discontinuity; there is a jump in tangential velocity and density on it.

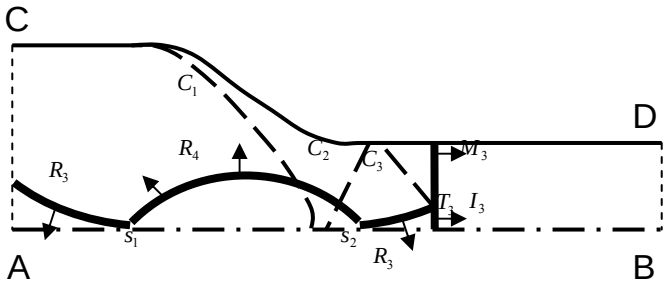

Fig. 8

Reflected shock wave R_3 is generated as result of the shock wave R_2 reflection from the wall. R_3 starts to interact with the incident shock wave. It produces the wave system $I_3\ M_3\ R_3\ C_3$. The wave system $I_3\ M_3\ R_3$ propagates in constant width plane channel therefore the shock waves I_3 and M_3 form almost flat front (fig.8). On fig. 8 the situation arising directly after reflection of the shock wave R_3 from the symmetry plane with formation of a wave R_4 is shown. Subsequently, the whole shock-wave flow structure consists of a "flat" wave, which is composed of two segments I_n and M_n, and a segment of the reflected shock wave R_n coming out of the triple point T_n, of an arc of a new reflected shock R_{n+1} and a sawtooth structure formed by the arcs of shock wave of the previous reflection stages: R_n, R_{n-1},…., R_2, R_1.

Experimental Results on Kelvin-Helmholtz instability.

Experimental results for a 130mm profile were conducted for an initial Mach number of M=1.33 and a color Schlieren visualization technique was used in all cases. Fig. 9 and 10 show the shock as it has just propagated through the profile reduction. It should be noted that a persistent instability arises only in the one bottom shear layer at a single point and not in the top. This fact has also been confirmed with additional testing using shadowgraph photography and flipping the top and bottom profiles. Thus, the cause of this instability has assumed to be triggered by either an inherent geometrical asymmetry in the system or unsteady flow conditions propagating behind the incident shock.

On the shock wave movement along a channel reduction, the longitudinal-transverse motion of the reflected waves R_i between the channel wall and the plane of symmetry occurs. As a result of multiple shock waves passage through the contact discontinuities C_i, intensification of shear flows along the contact surfaces occurs and the vorticity appears due to the baroclinic effect of divergence of pressure gradient at the shock front and the density gradient across the contact surface. Both these factors lead to the fact that in later time steps the reflected shear layers break down and form large Kelvin-Helmholtz instabilities.

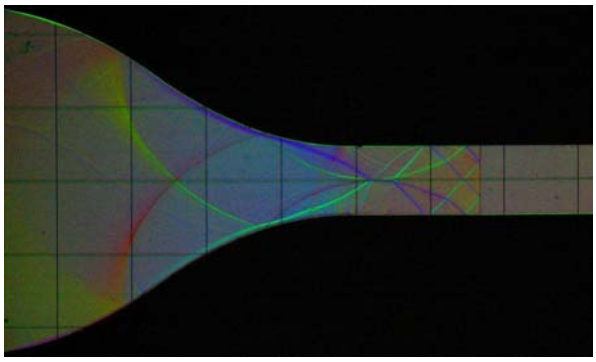

Fig. 9

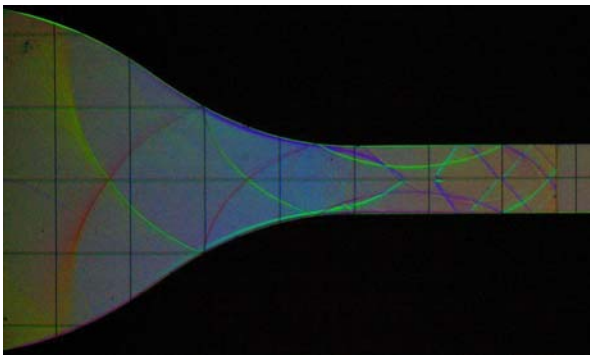

Fig. 10

CFD and experimental visualization comparison.

Fig. 11-13 presents the CFD results for the same conditions as on fig. 9, 10 (isolines of the Mach number and density of fields). The increased part of the computational domain in fig.10 near the contact surface C_1 is shown in fig. 13. Analysis of the results shows that the Kelvin-Helmholtz instability arises at the same time and in the similar points in the CFD calculations and in experiments.

Fig. 14 and 16 presents flow images in the reduced section for a similar incident shock of M=1.33. The results show earlier produced sets of shear layers breaking down into KHI, in fig. 16 this is quite intensive near the boundary. A front and rear facing jet on the center line of the first set of shear layers can be seen in fig. 14 and later in fig. 16. The front facing jet degrades far greater than the rear facing jet as is could be expected.

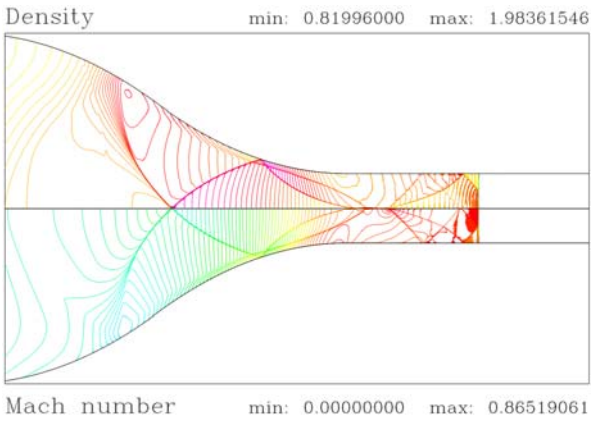

Fig. 11

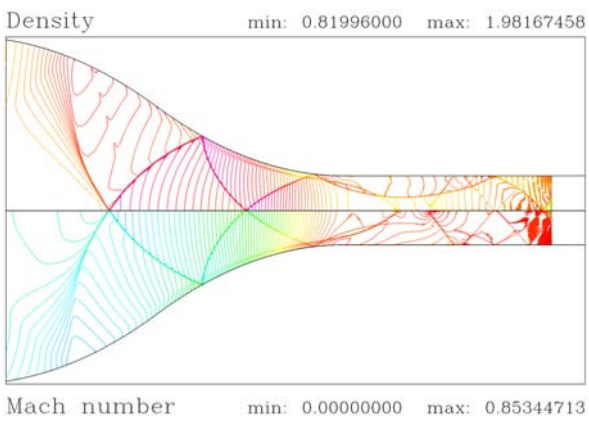

Fig. 12

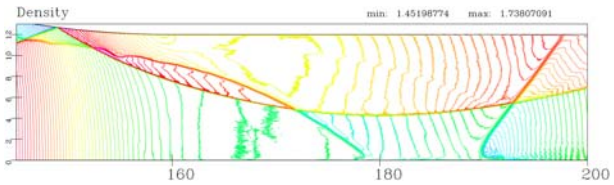

Fig. 13

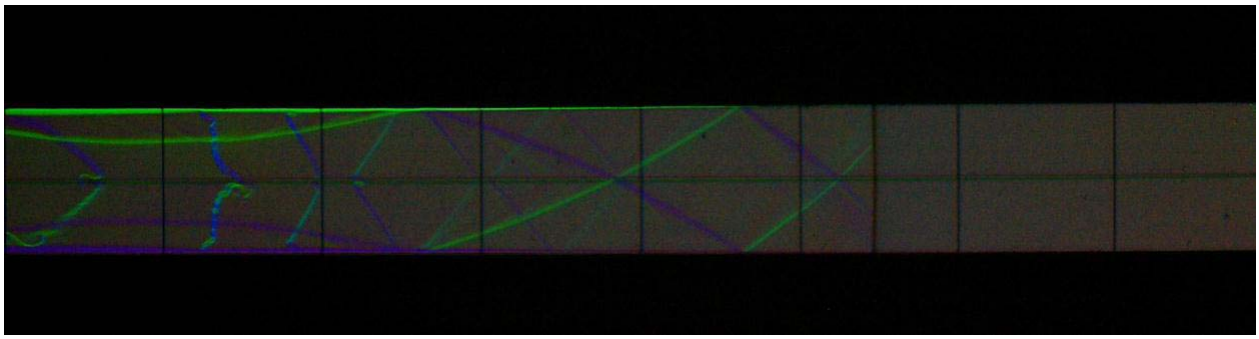

Fig. 14

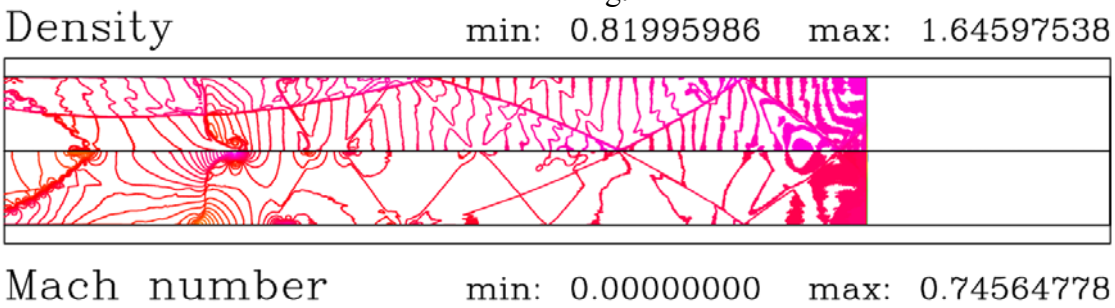

Fig. 15

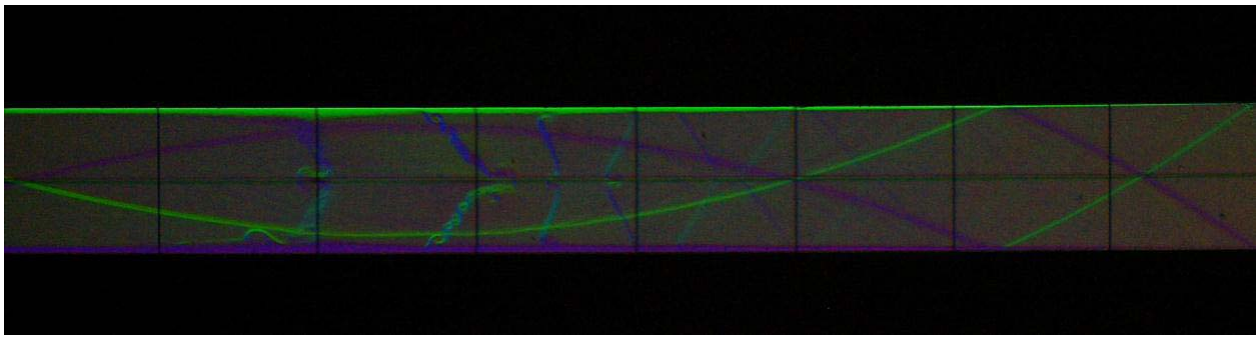

Fig. 16

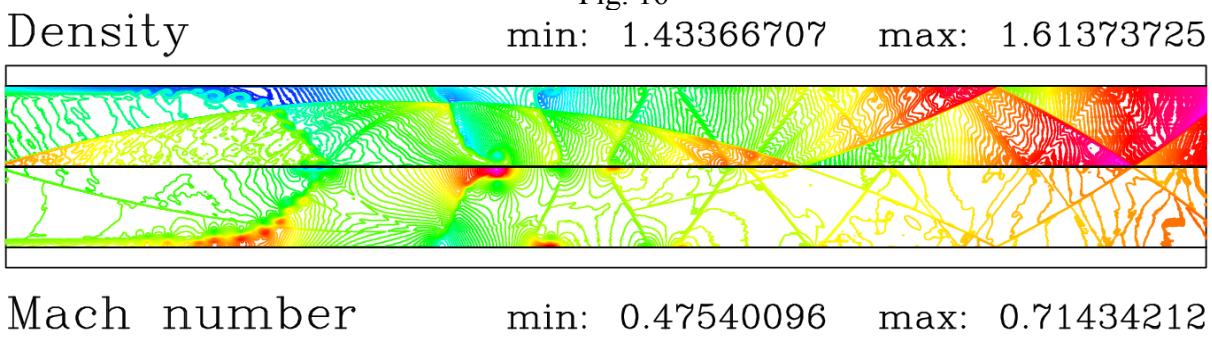

Fig. 17

The development of Kelvin-Helmholtz instability at the contact surfaces C_1 and C_2 in the later moments of time is shown in Fig.14-17.

Conclusions.

Detailed visualization (color shadow images) and high performance computing was conducted for the 2D analysis of the Kelvin-Helmholtz instability arising at shock interaction with curved channel profile with 80% area reduction. MUSCL approach was implemented with the Runge-Kutta third-order approximation in time. It was shown that KHI arises at the same time and in the similar points in the CFD calculations and in experiments the procedure of the spatial reconstruction of fifth-order accuracy in conjunction was used.

Acknowledgment. The work was supported by Joint Research NRF /RFBR grant 11-07-93959.

References

[1] J.N. Dowse, B.W. Skews. Area change effects on shock wave propagation. Proceedings of the 28th International Symposium on Shock Waves (ISSW-28), Manchester, UK, 17-22 July 2011. (CD Rom Proceedings 2840.pdf)

[2] T.V. Bazhenova and L. G. Gvozdeva, Unsteady Interactions of Shock Waves [in Russian], Nauka, 1977. 274 p.

[3] Ben-Dor G. Shocк wave reflection phenomena. NY: Springer–Verlag, 1992. 307 p.

[4] Ben-Dor G., Igra O., Elperin T. Handbook of shock waves. Vol. 2. San Diego: Academic Press, 2001. 792 p.

[5] A.N. Semenov M.K. Berezkina I.V. Krassovskaya //Tech. Phys. 54 (4), 491-496, 2009.

[6] Glushko G. S., Ivanov I. E., Kryukov I. A. Computational Method for Turbulent Supersonic Flows ISSN 2070_0482, Mathematical Models and Computer Simulations, 2010, Vol. 2, No. 4, pp. 407–422.

[7] Ivanov I, Kryukov I., Orlov D., Znamenskaya I. Investigations of shock wave interaction with nanosecond surface discharge Experiments in Fluids, 2010, Vol. 48, Is.4, P. 607-613.

[8] Ivanov IE, Kryukov IA, Semenov VV (2007) Numerical simulation of separated flow in nozzle with slots. Proceedings of the 26th international symposium on shock waves Gottingen, Germany July 2007 Part XIII Nozzle Flow. p 3810.

[9] Shu C-W, Osher S (1988) Efficient implementation of essentially non-oscillatory shock-capturing schemes. J. Comp. Phys. 77:439–471

[10] Woodward P, Colella P (1984) The numerical simulation of two-dimensional fluid flow with strong shocks. J. Comp. Phys. 54:115–173.